Optimized Dosing and Delivery of Bacteriophage Therapy for Wound Infections

Yung-Hao Lin[1*], Tejas Dharmaraj[2*], Qingquan Chen[2*], Arne Echterhof[2,3], Robert Manasherob[4], Lucy J. Zhang[5], Cas de Leeuw[6], Nana A. Peterson[2], Whitney Stannard[2], Zhiwei Li[2], Maryam Hajfathalian[2,7], Aviv Hargil[2], Hunter A. Martinez[2], Julie Pourtois[8], Tony H. W. Chang[2], Francis G. Blankenberg[9], Derek Amanatullah[4], Ovijit Chaudhuri[10#], and Paul L. Bollyky[2#]

[1]Department of Chemical Engineering, Stanford University, Stanford, CA, USA
[2]Division of Infectious Diseases and Geographic Medicine, Department of Medicine, Stanford University, Stanford, CA, USA
[3]Institute of Medical Microbiology, University Hospital of Muenster, Muenster, Germany
[4]Department of Orthopaedic Surgery, Stanford Hospital and Clinics, Redwood City, CA, USA
[5]Department of Material Science and Engineering, Stanford University, Stanford, CA, USA
[6]Institute for Molecules and Materials, Radboud University, Nijmegen, Netherlands
[7]Department of Biomedical Engineering, New Jersey Institute of Technology, University Heights, Newark, NJ
[8]Department of Biology, Stanford University, Stanford, CA, USA
[9]Division of Pediatric Radiology and Nuclear Medicine, Department of Radiology, Lucile Packard Children's Hospital, Stanford, CA, USA
[10]Department of Mechanical Engineering, Stanford University, Stanford, CA, USA

[*] Authors contributed equally
[#] Address correspondence to pbollyky@stanford.edu and chaudhuri@stanford.edu

Abstract

Lytic bacteriophages, viruses that lyse (kill) bacteria, hold great promise for treating infections, including wound infections caused by antimicrobial-resistant *Pseudomonas aeruginosa.* However, the optimal dosing and delivery strategies for phage therapy remain unclear. In a mouse wound infection model, we investigated the impact of dose, frequency, and administration route on the efficacy of phage therapy. We find that topical but not intravenous delivery is effective in this model. High-doses of phage reduces bacterial burden more effectively than low-doses, and repeated dosing achieves the highest eradication rates. Building on these insights, we developed "HydroPhage", a hyaluronan-based hydrogel system that uses dynamic covalent crosslinking to deliver high-titre phages over one week. HydroPhage eradicates infections five times more effectively than intravenous injection. We conclude that hydrogel-based sustained phage delivery enhances the efficacy of phage therapy and offers a practical, well-tolerated option for topical application.

Introduction

Chronic wounds are frequently complicated by antimicrobial-resistant (AMR) infections[1], with *Pseudomonas aeruginosa (Pa)* implicated in 25-50% of chronic infected wounds[2–5]. *Pa* strains in chronic wounds are frequently multidrug-resistant (MDR)[6–13]. Indeed, MDR-*Pa* is recognized as a serious threat by the Centers for Disease Control and Prevention (CDC) and the World Health Organization (WHO)[14,15], with few conventional antibiotics in development[16]. Hence, there is a need to pursue alternative therapies, including phage therapy (PT).

Bacteriophages (phages), viruses that infect and kill bacteria[19], are a promising alternative to treat bacterial infections. PT offers several advantages, including targeted activity against bacterial pathogens[17], biofilm disruption[18], and favorable safety profiles[19–22]. Numerous reports highlight the success of PT in treating MDR-*Pa* infections[23–25]. However, despite progress in phage pharmacology[26,27], the optimal dosing and route of administration for PT remains unclear.

Unfortunately, few studies are available to guide PT dosing and administration. While an older body of literature exists, much of it is heterogenous, written in languages other than English, and pre-dates the current era of PT[28]. More recent studies involving phage administration in mice have been conducted, but they often involve single-dose therapy in healthy (uninfected) animals[29]. There are suggestions that intravenous (IV), intraperitoneal (IP), and per oral (PO) administration may fail to deliver high concentrations of phages to endpoint tissues[30,31]. Although phages can replicate at the site of infection ("active killing")[32,33], the contribution of this to bacterial eradication is unclear[28]. While topical application of phages can be successful in preclinical models[34–36], optimal dosing and delivery methods remain unknown. Rigorous, systematic studies in animal models of infection are needed to guide the development of PT for different indications.

For most indications, PT in humans is typically administered intravenously[37], though local delivery is advised whenever possible[38]. However, appropriate dressing materials for topical phage delivery are lacking[38–42]. In humans, locally administered phage treatments for chronic wounds have primarily been delivered via gauze or cellulose wound dressings soaked with phages, without fully understanding the phage release kinetics from the dressings, and the success of these approaches has been variable[38–42]. Better approaches for controlled local phage delivery are needed.

Here, using an established mouse model of extended wound infection[43–45] that we have adapted for PT studies, we investigated the optimal route and dosing requirements for phage administration to treat infected wounds, and designed a phage-delivering hydrogel to meet these needs (**Fig. 1a**).

Results

Establishing a murine PT model.

We adapted the delayed inoculation model of wound infection to study PT[43–45]. This model involves wounding on Day -2, followed by inoculation with a luminescent strain of *Pa,* Xen41[46], on Day -1 under an occlusive dressing (Tegaderm) to prevent contamination. By allowing a provisional wound matrix to form before inoculation, this model enables stable *Pa* colonization without the need for foreign material or immune suppression. PT was then introduced to established infections one day after inoculation, on Day 0. An overview of this protocol is shown in **Figure 1b**.

We selected a phage with high activity against Xen41 by evaluating phages PAML-31-1, LPS-5, and Luz24 using planktonic suppression assays (PSA) and semi-solid substrate tests **(Extended Data Fig. 1a)**. Among them, PAML-31-1 **(Fig. 1a)**, demonstrated the strongest suppression of Xen41, with the highest "Suppression Index" (SI%)[47] – the percentage of growth inhibition caused by phage treatment within the first 48 hours of exposure **(Extended Data Fig.**

1b-g) in the PSA and the best performance in the semi-solid substrate test **(Extended Data Fig. 1h)**. Therefore, PAML-31-1 was selected for further studies.

We then identified the appropriate Xen41 inoculum required to establish an infection by inoculating mice with varying bacterial loads. A density of 5 x 10^5 CFU/wound was identified as the minimum dose required to achieve a 100% infection rate **(Fig 1c, d)**. Bacterial colony-forming units (CFU) were closely correlated with luminescent flux *in vitro* (**Fig. 1e)** and *in vivo* **(Fig. 1f)**. Despite the high infection rate, the model showed 100% survival **(Fig. 1g)** and minimal weight loss in mice **(Fig. 1h)**.

This robust preclinical model allowed for the assessment of PT efficacy using real-time BLI monitoring and endpoint culture-based methods. These included daily bacterial killing rate (percentage of wounds with BLI below limit of detection, LoD), persistent regrowth rate (percentage of wounds with BLI flux remained irreversibly above LoD), and endpoint eradication rate (percentage of wounds with CFU/mg below LoD) **(Fig. 1i–k)**.

Intravenous PT is ineffective against wound infections

We then investigated the efficacy of IV PT. As per the protocol in **Figure 1b**, mice were wounded, inoculated, and treated the following day with either topical PBS or PAML-31-1 administered IV via the dorsal penile vein **(Fig. 1l).** While IV phage treatment showed significant bacterial suppression as measured by BLI flux compared to PBS **(Fig. 1m)**, culture-based assays showed no significant reduction in CFU/mg tissue at the study endpoint **(Fig. 1n)**, despite substantial presence of phage in homogenized wound tissue **(Fig. 1o)**. Both PBS and IV phage injection led to only 5-6% eradication of *Pa* from murine wounds **(Fig. 1p)**. These results indicate that IV PT is ineffective at treating established wound infections.

Localized phage delivery reduces bacterial burden in infected wounds

We next investigated whether local delivery of phages at high titres could effectively treat wound infections. Mice received either a single high-dose (HD, 1 x 10^{11} PFU/mL, 40 µL) or a single low-dose treatment (LD, 2.5 x 10^{10} PFU/mL, 40 µL) **(Fig. 2a, b)**. In a third treatment group, the low-dose was administered daily (DD, 2.5 x 10^{10} PFU/mL/day, 40 µL, 4 days).

Local phage treatment significantly reduced bacterial burden and eradicated infections compared to PBS. BLI data showed that HD resulted in significantly lower flux compared to LD on Day 3 **(Fig. 2c)** and non-significant improvement of DD compared to LD **(Fig. 2d).** Flux measurements over time suggested initial bacterial suppression and gradual regrowth in later days **(Fig. 2e, f)**. Nonetheless, all of these treatments resulted in equivalent killing rates on Day 5, with a trend of DD being more effective than HD, which in turn was more effective than LD **(Fig. 2g)**.

Culture-based assays support the finding that eradication rates were not significantly different between treatments. However, there was a trend favoring repeated phage exposure from DD, with a 29% eradication rate versus 18% in the HD group, 16% in the LD group, and 6% in the PBS control group **(Fig. 2h).** LD, HD, and DD all resulted in significant but equivalent bacterial burden reduction compared to PBS, with 1.44-, 2.16-, and 2.20-log reductions in CFU/mg on Day 5, respectively **(Fig. 2i)**. The total amount of phage in wound homogenates at the study's endpoint was similar across treatment groups, regardless of dosage or frequency **(Fig. 2j)**.

Together, these results indicate that unlike IV delivery, topical PT promoted eradication of bacterial wound infection in this model. Further, higher doses and repeat dosing might be more effective at reducing bacterial burden. However, the emergence of resistance is common and equivalent with the topical treatment protocols evaluated here.

We also tested whether the *in vitro* phage selection assays could predict *in vivo* success by comparing the efficacy of HD PAML-31-1 and HD LPS-5. PAML-31-1 was significantly more effective than LPS-5 as predicted, with lower BLI fluxes and higher killing rates over time

(Extended Data Fig. 2a, b), supporting the utility of *in vitro* phage selection assays across multiple growth modes to infer *in vivo* efficacy.

Dual-crosslinked HA- and PEG-based hydrogels are injectable

While these studies highlight the efficacy of repeated and local delivery of high doses of phage, daily topical administration is not practical in most clinical settings. For example, the current standard of care at the Stanford Advanced Wound Care Clinic for chronic wounds involves once-weekly wound debridement. Therefore, we sought to develop hydrogels capable of sustained, local phage delivery for topical therapy. The ideal hydrogel for this application should be compatible with both phage and the wound milieu, injectable, and capable of delaying the diffusive release of phage to ensure that high titres are delivered over the course of one week.

To meet these criteria, we developed a soft, injectable hyaluronic acid (HA)- and polyethylene glycol (PEG)-based hydrogel for PT. This hydrogel is synthesized through a crosslinking mechanism involving covalent thioether bonds between hyperbranched PEG multi-acrylate (HBPEG) and thiolated hyaluronic acid (HA-SH) as well as dynamic covalent hemithioacetal bonds between 4-arm PEG-aldehyde or PEG-benzaldehyde crosslinkers (4ALD and 4BLD) and HA-SH **(Fig. 3a).** These reactions occur spontaneously under physiological conditions, avoiding the need for harsh solvents or catalysts. Lytic phages can be mixed with the polymer precursors prior to gelation, and the resulting phage-hydrogel is injectable through a fine needle **(Fig. 3b)**.

The combination of static covalent crosslinking (CC) and dynamic covalent crosslinking (DCC) results in a higher and more rapid increase in stiffness compared to hydrogels with CC or DCC alone **(Fig. 3c)**. In addition, the fast kinetics of the DCC enables immediate enhancement of viscosity and adhesiveness without compromising injectability **(Extended Data Fig. 3a, b).** These features ensure precise application and secure adherence of the hydrogels to the irregular contours of infected wounds. This HA-PEG hydrogel's unique properties make it highly suitable and easy to use for delivering therapeutic agents to wound beds.

HA-PEG hydrogels enable sustained release of high-titre phages

We next examined the release kinetics of phages from HA-PEG hydrogels *in vitro*, beginning with PAML-31-1. Hydrogels were formed in transwell inserts, immersed in a minimal amount of buffer, and the phage titre from the combined basolateral and apical chambers was measured using standard lytic plaque assays. The transwells were then transferred to a new well containing fresh buffer **(Fig. 3d)**.

To meet clinical needs, we optimized our hydrogel formulation for sustained phage release over one week. Prior work showed that hydrogels formed via thiol-Michael addition require polymer degradation mechanisms such as protease-cleavable crosslinkers to facilitate phage release[48]. We hypothesized that a lower thioether crosslinking density might enhance phage release by creating a looser polymer mesh, eliminating the need for additional polymer degradation mechanisms. Indeed, lower HBPEG concentrations increased phage recovery, suggesting that denser covalent thioether crosslinks trap phages and limit their release **(Fig. 3e and Extended Data Fig. 4a, b)**. Further investigations into hydrogels with low thioether crosslinking (1 mg/mL HBPEG) revealed that higher concentrations of 4ALD and 4BLD crosslinkers improved phage recovery **(Fig. 3f)**. At high concentrations of 4ALD and 4BLD, a lower percentage of benzaldehyde (%BLD) crosslinkers corresponded to higher percent phage recovery and more sustained release from day 4 to 7, likely due to more stable polymer-polymer and polymer-phage interactions with benzaldehyde compared to aldehyde. Thus, we identified that the optimal HA-PEG hydrogel formulation for sustained phage release was 5 mg/mL HA-SH, 1 mg/mL HBPEG, and 75 mg/mL of 4-arm PEGs with 10% 4BLD and 90% 4ALD, which was used for the remainder of the study.

Next, we assessed how phage titre and identity affected release kinetics. Higher encapsulated phage titres increased recovery; encapsulating 10^{11} PFU/mL in HP resulted in 62% phage recovery, compared to 28% recovery for 10^{10} PFU/mL and 21% recovery for 10^{9} PFU/mL **(Fig. 3g)**. Higher titres may saturate the binding of aldehyde and benzaldehyde groups, allowing a larger portion of unbound phages to diffuse freely. Testing three different *Pa*-targeting phages (Luz24, PAML-31-1, and LPS-5) revealed comparable release kinetics **(Fig. 3h)**. Unlike an ionically crosslinked alginate (AG-Ca^{2+}) hydrogel, which exhibited a burst release of nearly all encapsulated phages within the first 24 hours, HP exhibited sustained high-titre phage release (~10^{9} PFU/mL or higher) for up to 7 days **(Fig. 3i)**.

Finally, we explored the mechanisms driving phage release. Although dynamic covalent imine bonds between phage surface amines and aldehyde/benzaldehyde groups could theoretically sustain phage release from HP[49–51], and benzaldehyde groups are expected to form bonds with higher affinity than aldehyde groups[62,63], varying the ratio of aldehyde to benzaldehyde had little effect on phage release. Instead, polymer mass loss was closely correlated with phage release **(Fig. 3j)**, suggesting that hydrolytic erosion is the primary mechanism of phage release. Overall, our dual-crosslinked HA-PEG hydrogel offers a novel approach for sustained high-titre phage delivery.

HP disrupts *Pa* biofilms

We conducted *in vitro* tests to assess the antibacterial properties of HP. For HP encapsulating 10^{11} PFU/mL, the amount of PAML-31-1 released on Day 7 suppressed 30% of planktonic *Pa*, highlighting the extended antibacterial effect **(Fig. 4a)**. This prolonged suppression underscores the dose-dependent nature of phage-bacterial interactions and the potential of HP to control bacterial burden over extended timeframes *in vivo*.

Next, we evaluated if PAML-31-1 could escape HP and lyse *Pa* on a semi-solid substrate without fluid. On Mueller-Hinton agar plates inoculated with *Pa*, HP increased the zone of inhibition (ZOI) by 60% compared to a control gel, showing that phages could escape HP under drier conditions and propagate beyond the area in direct contact with HP **(Fig. 4b, c)**.

We also tested HP's efficacy against biofilms, which are dense polymeric matrices that harbor active and dormant bacterial populations, are prevalent in chronic wounds[52,53], and diminish the efficacy of antimicrobials, complicating treatment[54–58]. Biofilms of PAO1-GFP were grown on top agar and treated with PAML-31-1 in media, HP, or a control gel in a transwell insert after 24 hours. Both PAML-31-1 and HP reduced biofilm thickness by 43% and 52%, respectively, at 21 hours post-treatment, with no disruption of biofilm growth observed with the control gel or untreated samples **(Extended Data Fig. 5a)**. Biofilm density also decreased by 57% with PAML-31-1 and 65% with HP, while the control gel and untreated control exhibited increases in biofilm density of 55% and 72%, respectively **(Fig. 4d)**. Confocal microscopy vividly illustrated marked to complete disruption under treatment with PAML-31-1 and HP **(Fig. 4e, f and Extended Data Fig. 5b)**. Together, these results demonstrate that HP effectively suppresses and disrupts *P*a under both planktonic and biofilm conditions.

Localized HP clears wound infection more effectively than IV injection

Next, we compared the efficacy of HP versus systemic (IV) phage administration, hypothesizing that localized treatment would more effectively clear wound infections. Mice received either HP as a topical treatment or IV phage injection, with the same total amount of phage administered **(Fig. 4g, h)**. Daily measurements of killing rate indicate that HP was more effective than IV phage injection **(Fig. 4i)**, with a 40% killing rate by Day 5 post-treatment compared to just 6% for IV treatment **(Fig. 4j)**. Culture-based assays demonstrated a similar improvement of HP relative to IV, consistent with the BLI measurements, with a 25% eradication rate for HP compared to just 5% for IV treatment **(Fig. 4k)**. HP-treated mice also achieved a >2-log reduction in CFU/mg wound tissue relative to PBS (2.15, n=20) compared to a <1-log

reduction in CFU/mg for IV-treated mice (0.72, n=20) **(Fig. 4l)**, despite similar phage levels in wound homogenates at the end point **(Fig. 4m)**.

These results demonstrate the superior efficacy of HP in reducing bacterial burden and eradicating infections compared to systemic therapy, and highlight the merit of local, sustained delivery of high-titre phages via hydrogels.

Successful HP treatment partially restores the local inflammatory environment

We next assessed the skin immune response to *Pa* wound infection and its alteration by HP treatment. Using a 13-color flow cytometry panel **(Extended Data Table 1)**, we quantified the abundance of natural killer (NK) cells, neutrophils, macrophages, B cells, and T cells, while excluding monocytes, monocyte-derived dendritic cells (MoDCs), and conventional dendritic cells (cDCs) based on the gating strategy shown in **Extended Data Fig. 6**. Subpopulations of innate lymphocytes were not further discriminated. *Pa* infection significantly increased $CD45^+$ cells, NK cells, and non-significantly increased neutrophils, while reducing T cells **(Fig. 5a)**. Successful treatment with HP partially reversed some of these effects, reducing the proportions of $CD45^+$ cells, NK cells, and neutrophils following successful bacterial eradication **(Fig. 5b)**.

We also evaluated the biocompatibility and immunogenicity of the HA-PEG hydrogel and PAML-31-1 using RAW264.7 murine macrophage-like cells grown *in vitro* **(Fig. 5c)**. Neither the control gel nor PAML-31-1 exhibited any cytotoxicity **(Fig. 5d)** or induced M1/M2 polarization **(Fig. 5e-h)**.

These findings suggest that the HA-PEG hydrogel is biocompatible and nonimmunogenic, further supporting the suitability of HP for *in vivo* use.

Resistance to PAML-31-1 develops independently of treatment dosage, route, and efficacy

Despite the success of HP and DD in eradicating infections, eradication rates did not exceed 30% **(Fig. 6a)**. We hypothesized that bacteria might develop resistance against phages if not fully eradicated, similar to behavior seen *in vitro* **(Extended Data Fig. 1a)**. The positive correlation between phage and bacteria counts at the endpoint suggested that persistent bacterial burdens were not due to phage depletion **(Extended Data Fig. 7a, b)**.

To confirm the development of resistance to PAML-31-1 *in vivo* in response to phage treatments, we re-challenged stationary phase bacterial isolates from previous *in vivo* treatments with PAML-31-1 **(Fig. 6b)**. Bacterial isolates from all phage-treated groups showed significant reductions in SI% upon re-challenge compared to phage-unexposed wild-type Xen41 and PBS control groups, indicating that substantial regrowth of resistant bacteria had occurred, even with ineffective treatments such as IV injection **(Fig. 6c)**. The comparable SI% among resistant isolates across treatment groups suggests that the degree of resistance was independent of treatment efficacy.

We next assessed which treatments were most effective at preventing bacterial regrowth over time. For this, we compared the percentage of wounds with persistent bacterial regrowth, as assesssed from BLI measurements **(Fig. 1j)**. Interestingly, among localized treatments, only HP exhibited significantly suppressed bacterial regrowth compared to IV treatment **(Fig. 6d)**.

These results show that PAML-31-1 resistance develops regardless of treatment dosage, frequency, delivery route, and was not correlated with the reduction of bacterial burden. HP was the only treatment investigated capable of preventing persistent bacterial regrowth over time relative to systemic treatment.

Discussion

We have examined the dosing and administration requirements for PT in a mouse model of stable *Pa* wound infection. Our findings demonstrate that local, topical delivery is superior to IV delivery, higher doses are more effective than lower doses, and sustained delivery may offer

advantages in preventing regrowth. These findings provide experimental evidence supporting current guidelines that recommend high doses, repeated administration, and local PT when possible[37]. However, they also raise questions about the utility of IV therapy for treating wound infections.

Building on these insights, we developed "HydroPhage", a hydrogel system that delivers high-titre phages over one week. A single hydrogel treatment eradicates infections up to five times more effectively than IV delivery. Our results indicate that this delivery platform is non-immunogenic, biodegradable, and adaptable to wound treatment. These data highlight the significant potential of hydrogels in treating chronic wound infections, especially given the increasing prevalence of MDR pathogens like *Pa*.

The use of hyaluronan-based DCC hydrogels for phage delivery enables the sustained release of phage at high titres (i.e., $>10^9$ PFU/ml gel) over a week. Hydrogels are promising as wound dressings and platforms for controlled topical phage delivery[59–61]. However, the development of hydrogel-based topical phage delivery has lagged[62,63]. Previous hydrogel- or microparticle-based approaches for phage delivery often present either rapid burst release[35,49,64–67] or are clinically impractical due to low recovery of phage without mechanical (e.g., shaking) or biochemical (e.g., protease activity) interventions[48,68,69]. DCC hydrogels, with their intrinsic viscoelasticity, injectability, and self-healing characteristics, have gained significant attention in many biomedical applications[49,70–72]. Among various DCC chemistries considered, hemithioacetal crosslinking is particularly suited for topical applications, as its rapid kinetics and high reversibility provide immediate enhancement of viscosity and shear-thinning behavior[73]. We leveraged these properties, combined with the stability of covalent thioether bonds, to develop an adherent, slow-gelling HA-PEG hydrogel. The low covalent thioether crosslinking density provides stability without trapping sub-micron scale particles like phages, and allows for slow erosion, enabling sustained release of phages from the hydrogel. Additionally, HP is easily injectable and can conform to the irregular contour of the wound bed, ensuring prolonged contact with the affected area. Both HP and PT were safe in the mouse infection model, and successful bacterial eradication reduced inflammation, further supporting the safety of both HP and PT[61,74–76]. We propose that HP offers an optimized and clinically practical way to deliver phages for treating MDR wound infections. We envision that PT should integrate into chronic wound care regimens in the form of an advanced dressing that delivers effective concentrations of phages over a sustained period.

Surprisingly, despite the clear advantage of topical over IV PT in our model, we found that phage PFU levels within the wound bed were equivalent between IV and topical treatments. This suggests that phage propagation within tissues may be insufficient for bacterial clearance and that phage delivery to the wound surface is important in this model.

Our results also highlight the challenge of phage resistance in PT and the limitations of phage monotherapy[77,78]. We observe bacterial regrowth to single PT within 72 hours both *in vitro* and *in vivo*, with eradication achieved in only a minority of cases, regardless of treatment approaches. While phage cocktail treatments[79] may overcome this resistance, such approaches involve a level of complexity that was out of the scope of this investigation.

The limitations of this study include the reliance on a single strain of *Pa* and a single phage for the murine model. It would be important to extend these findings to include other pathogens and phages, including polymicrobial infections and phage cocktails. The use of Tegaderm in this model was essential for delivering topical liquids (e.g., phages) and for preventing secondary infection of exposed wounds by environmental pathogens. However, by containing PT within the wound bed, this dressing may have blunted the potential advantage of repeated dosing or hydrogel-enabled sustained release. Similarly, the presence of adherent bacteria may have surreptitiously increased bacterial counts as assessed by luminescence. Nonetheless, the assays and models developed here can facilitate further investigations of PT. As configured, this model

provides unique insights into resistance dynamics throughout the treatment course with paired endpoint analyses.

We conclude that these studies experimentally establish key treatment principles for PT. They provide a path forward for effective PT by enabling local, sustained, high-dose phage delivery using hydrogels.

Methods

Phage propagation

Phages were propagated using methods previously established in the lab[80]. PAML-31-1, LPS-5, Luz24, and OMKO1 were propagated in *Pseudomonas aeruginosa* (*Pa*) strain PAO1. Early- to mid-log phase cultures were infected with phages to generate lysates from 300 mL cultures.

Phage purification using AKTA-FPLC system

Bacteria were removed by 3 rounds of centrifugation at 8000 x *g*, 10 min, 4ºC. Supernatants were filtered through a 0.22 µm polyethersulfone (PES) membrane filter (Corning, Cat. No. 431118). The supernatant was treated with 5 U/mL Benzonase Nuclease (Sigma-Aldrich, Cat. No. E8263) overnight to digest free DNA. Benzonase-treated lysates were then mixed with 3M KH_2PO_4 buffer (pH 7.0) in a 1:1 ratio in preparation for purification by fast protein liquid chromatography (FPLC). The FPLC-based virus purification was conducted with a CIMmultus OH 1 mL monolithic column with a 2 µm channel size (Sartorius BIA Separations, Ajdovščina, Slovenia). The washing, regeneration, performance test, and storage of the column was carried out according to manufacturer recommendations. The column was attached to an ÄKTA Pure FPLC (GE Healthcare Biosciences, Sweden) equipped with a P960 sample pump and analyzed with UNICORN 5.0 software (Cytiva Life Sciences, USA). All purification protocols were run at room temperature and all buffers and samples were filtered through a 0.22 µm PES membrane. 40-60 mL of the mixed sample was loaded onto a pre-equilibrated column with 1.5 M KH_2PO_4 loading buffer, pH 7.0. After sample loading, the column was washed with 10 column volumes of loading buffer to remove unbound particles. The elution of bacteriophage was performed using a linear gradient over 20 column volumes from 1.5 M to 20 mM KH_2PO_4. The fraction corresponding to the eluted phage was collected based on UV A280 measurement. We then dilute or perform buffer exchange on the eluted phages into Tris+Mg buffer (100 mM NaCl, 50 mM Tris-HCl, 8 mM $MgSO_4$, pH 7.50).

Phage characterization

The size and morphology of phages were assessed as was done previously using transmission electron microscopy (TEM) on a JEOL JEM1400 (JEOL USA Inc., Peabody, MA, USA) operating at 80 kV[80]. In brief, 5 µL of diluted phage solution was applied onto carbon-coated copper grids (FCF-200-Cu, Electron Microscopy Sciences, Hatfield, PA, USA). Following a 3-minute incubation, the grid was immersed in ddH2O and subsequently treated with 1% uranyl acetate for staining. After drying for 15 min, the sample was ready for TEM imaging.

Hydrogel preparation

For making HA-PEG hydrogel, thiolated hyaluronic acid (HA-SH, 450 kDa, Blafar Ltd), hyperbranched PEG multi-acrylate (HBPEG, 10 kDa, Blafar Ltd), 4-arm PEG-aldehyde (4ALD, 10 kDa, CreativePEGWorks), and 4-arm PEG-benzaldehyde (4BLD, 10 kDa, SINOPEG) were reconstituted in PBS+Mg (Phosphate-Buffered Saline + 8 mM $MgSO_4$, pH 7.50) at concentration of 1wt%, 5wt%, 40 mM, and 40 mM respectively, adjusted to neutral pH, purged with argon gas

and kept on ice before use. Appropriate volumes of the following reagents were added into an Eppendorf tube in the order of: PBS+Mg, HBPEG, 4BLD, 4ALD to make a crosslinker mixture. Next, phage was added to the crosslinkers and vortexed, then HA-SH was added, vortexed again, and mixed thoroughly by pipetting. The viscous slow-gelling mixture then was withdrawn by pipette to deposit into transwell inserts (Corning, USA, Cat. No. 353492) for *in vitro* assays or by insulin syringe with a 28G needle (BD, REF. 329461) to inject for *in vivo* treatment. The final formulation of HA-PEG hydrogel was 5 mg/mL HA-SH, 1 mg/mL HBPEG, 75 mg/mL of 4-arm PEGs with 10% 4BLD and 90% 4ALD, and 10^{11} PFU/mL phage unless otherwise noted.

For making the ionically crosslinked alginate hydrogel (AG-Ca^{2+}), lyophilized alginate (PRONOVA UP VLVG, IFF, USA) was reconstituted in Tris+Mg buffer (50 mM Tris-HCl, 100 mM NaCl, 8 mM $MgSO_4$) at 4wt%. Calcium sulfate was prepared as a form of saturated slurry in deionized water at 500 mM. Reconstituted alginate and phage solution were added to a 1 mL syringe, and the calcium slurry was added into another syringe using a pipette. The solution in each syringe was thoroughly mixed by moving the plunger up and down before the syringes were connected with a Luer Lock. Alginate, calcium, and phages were then mixed thoroughly between syringes and 100 µL was deposited into a transwell insert. The formulation of the AG-Ca^{2+} hydrogel was 2wt% alginate, 50 mM calcium, and 10^{11} PFU/mL phage. Detailed polymer information was included in **Extended Data Table 3**.

Transwell-release assay

Transwell inserts for 24-well plates were blocked in a solution of 2% bovine serum albumin (BSA) in PBS for 1 hour, rinsed with PBS+Mg for 10 min, thoroughly aspirated, and then air-dried for 20 min at room temperature prior to use. 100 µL of hydrogel with encapsulated phage was aliquoted into each transwell insert and incubated in a closed box at room temperature for 3.5 hours until the hydrogels had fully gelled. After gelation, transwells were transferred to 24-well tissue culture-treated plates (Corning, NY, USA, Cat. No. 3524) containing 500 µL of PBS+Mg buffer. An additional 200 µL of PBS+Mg was added on top of the hydrogel to prevent drying. After 24 hours of incubation at 37°C, the transwell insert with hydrogel was removed. The buffer on top of the hydrogel and any residual buffer on the bottom of the transwell were carefully collected and combined with the buffer in the 24-well plate and stored at 4°C for phage titre quantification. The transwell was transferred into a new well containing 500 µL of fresh buffer, and 200 µL of fresh buffer was added on top. This process was repeated for 7 days.

HA-PEG hydrogel erosion

The erosion study on HA-PEG hydrogel without phage encapsulation was conducted by forming hydrogels in the transwell insert, submerging in PBS+Mg buffer, and transferring daily as described above. The dry mass of the hydrogel was measured at each time point after lyophilization. Erosion, defined as the percentage to maximum polymer mass loss, was quantified as the loss of dry mass at each time point normalized to the endpoint of the assay on Day 7.

Plaque assays

Phages were enumerated by plaque assays using the spot dilution double-agar overlay technique. 100 µL of mid-log phase bacteria was added to 5 mL of top agar (5 g/L agar, 10 g/L tryptone, 10 g/L NaCl, 20 mM $MgSO_4$, 20 mM $CaCl_2$) and poured onto LB-agar plates to solidify. 10-fold serial dilutions of phages were prepared in 96-well polystyrene U-bottom tissue culture-treated plates (ThermoFisher Scientific, Waltham, MA, USA, Cat. No. 168136) in SM buffer (50 mM Tris-HCl, 100 mM NaCl, 8 mM $MgSO_4$, 0.01% gelatin (Sigma-Aldrich, USA, Cat. No. G7041), pH 7.50). 10 µL of each dilution was spotted onto the top agar, incubated at 37°C overnight, and plaques were counted.

Planktonic suppression assay (PSA)

Overnight cultures were prepared from a glycerol stock of Xen41 or from cryopreserved mice wound isolates by directly inoculating LB medium and incubating at 37°C with shaking at 200 x *rpm* overnight. A 50 µL aliquot of diluted overnight culture in "modified-LB" (LB buffer + 50 mM Tris-HCl + 8 mM $MgSO_4$, pH 7.50) was prepared at the concentration of 3.75 x 10^7 CFU/mL in a 96-well plate. 100 µL of phage suspension in modified-LB was added to each well containing bacteria to reach the target MOI in a total volume of 150 µL. Wells were then topped with 15 µL of mineral oil and covered with a gas-permeable sealing membrane to prevent evaporation (USA Scientific, Cat. No. 9123-6100). The final co-cultures were incubated at 37°C in an automated spectrophotometer (Biotek Synergy 2, Agilent Technologies, USA) for 48 hours, with OD600 measurements taken every 20 min following 5 seconds of shaking. The control consisted of bacteria incubated with modified-LB without phages. Each sample was prepared in triplicate. The Suppression Index (SI%) was calculated using the formula provided below to quantify the relative suppression of bacterial growth in phage-treated versus non-treated condition[47].

$$Suppression\ Index\ (\%)\ =\ \frac{AUC_{48h}\ non\text{-}treated\ -\ AUC_{48h}\ phage\text{-}treated}{AUC_{48h}\ non\text{-}treated}$$

$$AUC\ =\ area\ under\ the\ curve$$

To evaluate the efficiency of different phages to suppress planktonic Xen41, an MOI of 8,000 was compared. To evaluate the resistance of mouse isolates to PAML-31-1 phage, suppression was tested at an MOI of 500. Phage titres were measured using plaque assays against *Pa* PAO1.

Zone of inhibition (ZOI) assay

An overnight culture of PAO1 was subcultured to an OD600 of 0.65, then 100 µL was spread onto a Mueller-Hinton agar plate and air-dried. 100 µL of pre-formed HA-PEG hydrogel (5 mg/mL HA-SH, 1 mg/mL HBPEG, 75 mg/mL of 4-arm PEGs with 10% 4BLD and 90% 4ALD, and 10^{11} PFU/mL PAML-31-1 phage) was transferred onto the inoculated agar plate after 3.5 hours of gelation. The hydrogel was allowed to seal with the agar surface for 15 min, before inverting and incubating at 37°C for 24 hours. The zone of inhibition (ZOI) was measured.

***In vitro* biofilm assay and confocal microscopy**

The overnight culture of PAO1-GFP was diluted to OD600 of 0.05 in tryptic soy broth (TSB) and kept on ice. 250 µL of top agar was solidified in each glass bottom 24-well plate (Cellvis, USA, Cat. No. P24-1.5H-N) before adding 300 µL of inoculum. The inoculum was allowed to adhere for 30 min in the incubator at 37°C, after which the media was gently replaced with 500 µL of fresh TSB. After 5 hours, each well was replaced with 800 µL of fresh TSB and then incubated overnight. At 24 hours, each well was gently rinsed with 800 µL of PBS+Mg, then replaced with 300 µL of modified-LB, followed by adding treatments. The control treatment consisted of 200 µL of PBS+Mg, while phage treatment consisted of 200 µL of phage suspension at 10^{11} PFU/mL added directly into wells. Control gel treatment was 100 µL of HA-PEG gel in transwell insert topped with 200 µL of PBS+Mg, and HydroPhage (HP) treatment was 100 µL of HA-PEG gel containing PAML-31-1 at 10^{11} PFU/mL in a transwell insert topped with 200 µL of PBS+Mg. Biofilms were monitored with a laser-scanning Leica SP8 confocal microscope with a 25x 0.95-NA water immersion objective at 0, 3, 8, and 21 hours. Biofilm density was quantified as the percentage of area with PAO1-GFP signal at the base of biofilm, the biofilm and agar interface, and biofilm density change was defined as the change of biofilm density at 21 hours normalized to the initial density of each sample. Due to the significant presence of planktonic bacteria and/or the

significant disruption of biofilm from treatments, biofilm thickness was manually defined from the media-biofilm boundary to the base of the biofilm, as determined by x-z and y-z projections. 3D rendering of the biofilm was reconstructed with Imaris imaging software (Oxford Instruments).

In vitro cytotoxicity and activation of hydrogel against RAW264.7 macrophages

A transwell exposure assay was used to measure the cytotoxicity and immunogenicity of pre-formed hydrogels against RAW264.7 murine macrophage-like cells **(Extended Data Fig. 6a)**. RAW264.7 cells were grown to passage 6 post-thaw in complete DMEM (DMEM/F12 + 10% fetal bovine serum + 1% penicillin/streptomycin). 5 x 10^4 cells were seeded in 24-well tissue culture-treated plates. After overnight incubation, the media was replaced with 500 µL of fresh cDMEM. Cells were treated for 24 hours with one of the following: media only (negative control), 8% DMSO (positive cytotoxicity control), 1 µg/mL *Escherichia coli* lipopolysaccharide (M1 polarizing positive control; Sigma-Aldrich, Cat. No. L3024-5mg), 20 ng/mL mouse IL-4 (M2 polarizing positive control; ThermoFisher Scientific, USA, Cat. No. 214-14-1MG), FPLC-purified PAML-31-1 at 5 x 10^9 PFU/mL, or 100 µL of pre-formed hydrogels in transwell inserts, with 200 µL of fresh media added on top to prevent drying. After 24 hours of incubation, the media was removed, and cells were rinsed once with PBS. Cells were then stained with 300 µL of 1:3000 IRDye 800CW in PBS for 15 min at room temperature. Staining was quenched by the addition of 1 mL ice-cold FACS buffer. After centrifugation, cells were resuspended in 300 µL of anti-mouse CD16/32 (Fc block) in FACS at a concentration of 1 µg/million cell for 10 min at 4°C. After centrifugation and removal of excess Fc block, samples were stained with antibodies **(Extended Data Table 2)** for 20 min at 4°C in a staining volume of 300 µL. Samples were rinsed twice in ice-cold FACS and fixed in 500 µL 10% neutral buffered formalin (ThermoFisher Scientific, USA, Cat. No. 9990245) for 15 min at room temperature. Cells were scraped and transferred to a 96-well V-bottom plate for analysis by flow cytometry within one week.

In vitro and *in vivo* bioluminescence to CFU (BLI-CFU) correlation

Quantification of bacterial wound infections using luminescent strains of *Pa* was performed as described previously[43]. In brief, a dilution series of *Pseudomonas aeruginosa* Xen41 (PerkinElmer, MA, USA) was prepared in a black 96-well plate (ThermoFisher Scientific, USA, Cat. No. 165305) ranging from 10^0 to 10^7 CFU/well in a total volume of 100 µL. Samples were prepared in triplicate. CFU counts were verified by plating serial dilutions on nonselective LB agar plates. Bioluminescence imaging was performed on the Lago X *In Vivo* Imaging System (Spectral Instruments Imaging, USA), using the same settings described in the Methods section on "Bioluminescence Imaging". Linearity between bioluminescent flux ($\log_{10}$(photons/s)) and bacterial burden (CFU) were assessed for flux values above 4 and 5 for the *in vitro* and *in vivo* experiments, respectively.

Delayed treatment mouse infection model

Male C57BL/6J mice (#000664) were purchased from the Jackson Laboratory. All experiments and animal use procedures were approved by the Institutional Animal Care and Use Committee (IACUC) at the School of Medicine at Stanford University. The study design was adapted from previous work[81]. Briefly, 6-7-week-old male mice were anesthetized using 3% isoflurane and shaved. The shaved area was cleaned with povidone-iodine (Dynarex, USA, Cat. No. 1201) and isopropyl alcohol swabs. Mice received a single subcutaneous injection of slow-release buprenorphine (0.1-0.5 mg/kg, ZooPharm, USA) as an analgesic. A single circular midline dorsal full-thickness wound was created using a 6 mm biopsy punch (Integra Miltex, Catalog No.12-460-412). The wounds were immediately covered with Tegaderm (3M, USA, Cat. No. 1642W) and secured with silicone adhesive on the periphery (Vapon, USA, Cat. No. NTL1). Mice were placed in padded plastic collars (Saf-T-Shield, KVP International, USA, Cat. No. RCM) to prevent the removal of wound dressings. Mice received 500 µL of 0.9% normal saline by IP

injection on the wounding day and food pellets covered with veterinary nutrient supplements (California Veterinary Supply, USA, Cat. No. HS-10033).

On the infection day, *Pa* Xen41 was grown in LB at 37°C with shaking to mid-log phase. Bacteria were pelleted by centrifugation, resuspended in PBS, and diluted to 1.25 x 10^7 CFU/mL. The inoculum density was verified by plating serial dilutions on LB agar plates. 24 hours post-wounding, wounds were inoculated with 40 µL Xen41 under Tegaderm using an insulin syringe (28G) at 5 x 10^5 CFU/wound. Bioluminescence images were obtained 1 hour post-infection using the Lago X *In Vivo* Imaging System to confirm that the inoculum was properly injected under the Tegaderm.

24 hours post-infection ("Day 0"), all mice were imaged before the first treatment. Mice were treated with 1) PBS as control; 2) IV phage via dorsal penile vein injection, 1 x 10^{11} PFU/mL; 3) topical single high-dose (HD), 1 x 10^{11} PFU/mL; 4) topical single low-dose (LD), 2.5 x 10^{10} PFU/mL; 5) topical daily low-dose (DD), 2.5 x 10^{10} PFU/mL, for 4 days; or 6) topical HydroPhage (HP), 1 x 10^{11} PFU/mL. All mice were weighed daily. Additional Tegaderm dressings were applied on top of existing ones if the dressing became loose. Mice that completely removed the Tegaderm dressings or which partially removed and exhibited a resultant >2-log reduction in luminescent flux in a day, indicating potential drying of infection or treatment, were excluded from subsequent analysis. Six days post-infection, mice were euthanized, and the wound was harvested (1 cm^2). Each wound was bisected. One half was weighed, homogenized, and used for enumerating colony-forming units (CFU) and plaque-forming units (PFU), while the other half was processed for flow cytometry. The next day, at least 10 colonies from each wound isolate were picked, cultured overnight, and then stored in 30% glycerol at -80°C for further characterization, including quantification of phage resistance using PSA.

Bioluminescence imaging (BLI)

Bioluminescence imaging was performed on the Lago X *In Vivo* Imaging System (Spectral Instruments Imaging, USA). A series of exposures ranging from 5 s to 60 s were taken to determine the optimal exposure time. The longest exposure without overexposure was used for analysis. The following imaging settings were used: F-stop 1.2, Binning: Heavy, FOV: 25. Images were analyzed using Aura version 4.0 (Spectral Instruments Imaging, USA). Radiance (photons/s/cm^2/sr) within a manually selected region of interest (ROI) was integrated to measure total signal flux (photons/s).

Wound flow cytometry

Wounds were rinsed once in HBSS, blotted to remove excess HBSS, and placed into pre-weighed 1.5 mL polystyrene tubes containing 500 µL freshly prepared, ice-cold digestion buffer (RPMI-1640 + 25 mM HEPES, pH 7.4, 1.3 WU/mL Liberase TL (Roche, Switzerland, Cat. No. 05401020001), 2 U/mL bovine DNase I (Roche, Switzerland, Cat. No. 11284932001), 25 mM $MgCl_2$, 1 mM $CaCl_2$, 200 U/mL collagenase IV (Worthington Biochemical, USA. Cat. No. LS004188)[82]. Samples were weighed and minced finely using scissors. An additional 500 µL ice-cold digestion buffer was added to samples and incubated at 37°C with shaking at 750 x *rpm* for 2 hours. Samples were inverted several times every 30 min during the incubation. After the 2-hour digestion, samples were treated with 100 µL Accutase (Innovative Cell Technologies, San Diego, CA, USA, Cat. No. AT104) and incubated for 20 min at room temperature.

Digested samples were passed through a 40 µm nylon cell strainer (Corning, Corning, NY, USA, Cat. No. 352340) pre-wetted with 1 mL of ice-cold FACS buffer (PBS + 1 mM EDTA + 1% BSA). Samples were gently pressed through the strainer using the rubber end of a syringe plunger. Cell strainers were rinsed with 5 mL of ice-cold FACS buffer. Cells were pelleted by centrifugation (500 x *g*, 10 min, 4°C), and the supernatant was aspirated. Pellets were resuspended in 1 mL ice-cold FACS buffer and pelleted again. Pellets were resuspended in 250 µL of room temperature ACK red blood cell lysis buffer (0.15 M NH_4Cl, 10 mM $KHCO_3$, 0.1 mM EDTA, pH 7.3) and

incubated for precisely 4 minutes (variation <5 seconds), after which lysis was stopped by the addition of 750 µL of PBS.

Cells were then pelleted by centrifugation (500 x *g*, 20 min), removed supernatant, and resuspended in 200 µL ice-cold FACS buffer. 10 µL samples were diluted into a final volume of 200 µL and counted on a flow cytometer. 650,000 cells/sample were aliquoted to a 96-well V-bottom tissue culture-treated plate (Corning, Corning, USA, Cat. No. 07-200-96). The remaining cells were pooled and aliquoted for unstained, single-stained, and fluorescence-minus-one (FMO) controls.

For staining, cells were rinsed once in ice-cold FACS buffer and then stained in 50 µL 1:3000 IRDye 800CW Live/Dead NIR stain in PBS for 15 minutes at room temperature. Staining was quenched by the addition of 150 µL of ice-cold FACS buffer. After centrifugation, cells were resuspended in 30 µL of anti-mouse CD16/32 (Fc block) in FACS at a concentration of 1 µg/million cells for 10 min at 4°C. After centrifugation and removal of excess Fc block, samples were stained with antibodies (listed below) for 20 min at 4°C in a staining volume of 30 µL. Samples were then rinsed twice in ice-cold FACS and fixed in 200 µL 4% paraformaldehyde (20 min, room temperature). Samples were then resuspended in 200 µL FACS and acquired on the Cytek Aurora NL-3000 spectral flow cytometer (Cytek Biosciences, CA, USA) within 1 week of fixation. Spectral unmixing was performed using narrow gates and without unmixing autofluorescence.

Statistical analyses

Statistical analyses were performed using GraphPad Prism version 10, except for generalized linear mixed model with binomial distribution using R package. Ordinary one-way analysis of variance (ANOVA) with Tukey post-hoc tests was used for multiple comparisons unless otherwise noted. Unpaired two-tailed Student's *t*-tests were used for comparison between two groups unless otherwise mentioned. $P \leq 0.05$ was considered significant unless otherwise noted. Data were presented as mean with error bars representing the standard deviation (S.D.), unless otherwise noted. (* $P \leq 0.05$, ** $P \leq 0.01$, *** $P \leq 0.001$, **** $P \leq 0.0001$).

Acknowledgements

In vivo imaging was performed at Stanford Center for Innovation in *In Vivo* Imaging (Sci^3). We thank Drs. A. Khosravi, N. Nagy, A. Saraswathibhatla, and D. Indana and other members from the Bollyky and Chaudhuri labs for their scientific inputs; the staff at the Sci^3 for providing the support needed to perform the required experiments, including Dr. F. Habte. The research reported in this publication was supported by a Stanford Catalyst Grant and a Stanford Coulter Translational Grant. Q. C. discloses support from Cystic Fibrosis Foundation CHEN21F0, Cystic Fibrosis Research Institute, and Stanford Maternal & Child Health Research Institute. T.D. discloses support from Stanford University Medical Scientist Training Program National Institutes of Health grant T32-GM007365; Stanford Interdisciplinary Graduate Fellowship affiliated with Sarafan ChEM-H, Gold Family Graduate Fellow. M.H. discloses support from National Institutes of Health grants R00-EB028838 and K99EB028838. O.C. acknowledges support from NIH grants R01 AR081993 and R01 GM148535. P.L.B discloses support from National Institutes of Health grant R01 HL148184-01; National Institutes of Health grant R01 AI12492093; National Institutes of Health grant R01 DC019965; Cystic Fibrosis Foundation grant; Emerson Collective grant. The contents are those of the authors and do not necessarily represent the views of the funding agencies.

Author contributions

Y.H.L., T.D., and Q.C. contributed equally. Y.H.L., T.D., Q.C., R.M., D.A., O.C., and P.L.B. conceived the study. Y.H.L. and R.M. performed hydrogel phage release pilot studies. Y.H.L., T.D., and Q.C. designed the experiments and mouse model. Y.H.L. and L.J.Z. performed rheological tests, and Y.H.L. conducted hydrogel degradation studies. Y.H.L., T.D., Q.C., L.J.Z., A.E., C.D.L., and W.S. performed *in vitro* phage release studies. Y.H.L., A.E., and Z.L. performed *in vitro* phage selection and resistance assays, and Y.H.L. conducted biofilm studies. T.D., N.A.P., and H.A.M. performed the flow cytometry assays and *in vitro* macrophage cytotoxicity and activation studies. Q.C., T.D., A.E., Y.H.L., L.J.Z., F.G.B., and T.H.W.C. performed *in vivo* studies, with C.D.L, Y.H.L., and A.E. curating data. M.H. conducted TEM imaging. A.E., A.H., and T.D. propagated and purified phages. Y.H.L., Q.C., T.D., A.E., and J.P. analyzed and interpreted the data. O.C. and P.L.B. supervised the study. Y.H.L., T.D., Q.C., O.C., and P.L.B. wrote the manuscript. All authors reviewed the manuscript.

Competing interests

The authors declare no competing interests

References

1. Sen, C. K. *et al.* Human skin wounds: a major and snowballing threat to public health and the economy. *Wound Repair Regen* **17**, 763–71 (2009).

2. Kirketerp-Møller, K. *et al.* Distribution, organization, and ecology of bacteria in chronic wounds. *J Clin Microbiol* **46**, 2717–22 (2008).

3. Dowd, S. E. *et al.* Survey of bacterial diversity in chronic wounds using Pyrosequencing, DGGE, and full ribosome shotgun sequencing. *BMC Microbiol* **8**, 43 (2008).

4. Malic, S. *et al.* Detection and identification of specific bacteria in wound biofilms using peptide nucleic acid fluorescent in situ hybridization (PNA FISH). *Microbiology (N Y)* **155**, 2603–2611 (2009).

5. James, G. A. *et al.* Biofilms in chronic wounds. *Wound Repair and Regeneration* **16**, 37–44 (2008).

6. Kapel, N., Caballero, J. D. & MacLean, R. C. Localized pmrB hypermutation drives the evolution of colistin heteroresistance. *Cell Rep* **39**, 110929 (2022).

7. Olalekan, A. *et al.* High incidence of carbapenemase-producing *Pseudomonas aeruginosa* clinical isolates from Lagos, Nigeria. *JAC Antimicrob Resist* **5**, (2023).

8. Ogbolu, D. O., Piddock, L. J. V. & Webber, M. A. Opening Pandora's box: High-level resistance to antibiotics of last resort in Gram-negative bacteria from Nigeria. *J Glob Antimicrob Resist* **21**, 211–217 (2020).

9. Woodford, N., Palepou, M.-F. I., Babini, G., Bates, J. & Livermore, D. Carbapenemase-producing Pseudomonas aeruginosa in UK. *The Lancet* **352**, 546–547 (1998).

10. Khan, F., Khan, A. & Kazmi, S. U. Prevalence and susceptibility pattern of multi drug resistant clinical isolates of Pseudomonas aeruginosa in Karachi. *Pak J Med Sci* **30**, (2014).

11. Gill, J., Arora, S., Khanna, S. & Kumar, K. V. S. Prevalence of multidrug-resistant, extensively drug-resistant, and pandrug-resistant Pseudomonas aeruginosa from a tertiary level Intensive Care Unit. *J Glob Infect Dis* **8**, (2016).

12. Mohamed, M., Mohamed, H. & Afifi, M. Prevalence of MDR Pseudomonas aeruginosa in Intensive care units and burned patients. *Journal of Environmental Studies* **27**, (2022).

13. Liu, X. *et al.* Risk Factors for Multidrug-Resistant Organisms Infection in Diabetic Foot Ulcer. *Infect Drug Resist* **15**, (2022).

14. World Health Organization (WHO). *WHO Bacterial Priority Pathogens List*. *https://www.who.int/publications/i/item/9789240093461* (2024).

15. Centers for Disease Control and Prevention (CDC). Antibiotic Resistance Threats in The United States 2019. *https://www.cdc.gov/antimicrobial-resistance/data-research/threats/index.html* (2019).

16. Reig, S., Le Gouellec, A. & Bleves, S. What Is New in the Anti–Pseudomonas aeruginosa Clinical Development Pipeline Since the 2017 WHO Alert? *Front Cell Infect Microbiol* **12**, 1–16 (2022).

17. Fiedler, A. W. *et al.* Phage therapy minimally affects the water microbiota in an Atlantic salmon (Salmo salar) rearing system while still preventing infection. *Sci Rep* **13**, 1–13 (2023).

18. Kovacs, C. J. *et al.* Disruption of Biofilm by Bacteriophages in Clinically Relevant Settings. *Mil Med* **00**, (2023).

19. Burrowes, B., Harper, D. R., Anderson, J., McConville, M. & Enright, M. C. Bacteriophage therapy: potential uses in the control of antibiotic-resistant pathogens. *Expert Rev Anti Infect Ther* **9**, 775–85 (2011).

20. Maddocks, S. *et al.* Bacteriophage Therapy of Ventilator-associated Pneumonia and Empyema Caused by Pseudomonas aeruginosa. *Am J Respir Crit Care Med* **200**, 1179–1181 (2019).

21. Cano, E. J. *et al.* Phage Therapy for Limb-threatening Prosthetic Knee Klebsiella pneumoniae Infection: Case Report and In Vitro Characterization of Anti-biofilm Activity. *Clin Infect Dis* **73**, e144–e151 (2021).

22. Chan, B. K. *et al.* Phage treatment of an aortic graft infected with *Pseudomonas aeruginosa*. *Evol Med Public Health* **2018**, 60–66 (2018).

23. Karinja, S. J. & Spector, J. A. Treatment of Infected Wounds in the Age of Antimicrobial Resistance: Contemporary Alternative Therapeutic Options. *Plast Reconstr Surg* **142**, 1082–1092 (2018).

24. Kutter, E. *et al.* Phage Therapy in Clinical Practice: Treatment of Human Infections. *Curr Pharm Biotechnol* **11**, 69–86 (2010).

25. Abedon, S. T., Kuhl, S. J., Blasdel, B. G. & Kutter, E. M. Phage treatment of human infections. *Bacteriophage* **1**, 66–85 (2011).

26. Międzybrodzki, R. *et al.* Pharmacokinetic and Pharmacodynamic Obstacles for Phage Therapy From the Perspective of Clinical Practice. *Clinical Infectious Diseases* **77**, S395–S400 (2023).

27. Dąbrowska, K. Phage therapy: What factors shape phage pharmacokinetics and bioavailability? Systematic and critical review. *Med Res Rev* **39**, 2000–2025 (2019).

28. Dąbrowska, K. & Abedon, S. T. Pharmacologically Aware Phage Therapy: Pharmacodynamic and Pharmacokinetic Obstacles to Phage Antibacterial Action in Animal and Human Bodies. *Microbiology and Molecular Biology Reviews* **83**, (2019).

29. Nang, S. C. *et al.* Pharmacokinetics/pharmacodynamics of phage therapy: a major hurdle to clinical translation. *Clinical Microbiology and Infection* vol. 29 Preprint at https://doi.org/10.1016/j.cmi.2023.01.021 (2023).

30. Yip, Y. L., Hawkins, N. J., Smith, G. & Ward, R. L. Biodistribution of filamentous phage-Fab in nude mice. *J Immunol Methods* **225**, 171–178 (1999).

31. Lin, Y. W. *et al.* Pharmacokinetics/pharmacodynamics of antipseudomonal bacteriophage therapy in rats: a proof-of-concept study. *Clinical Microbiology and Infection* **26**, 1229–1235 (2020).

32. Tiwari, B. R., Kim, S., Rahman, M. & Kim, J. Antibacterial efficacy of lytic Pseudomonas bacteriophage in normal and neutropenic mice models. *The Journal of Microbiology* **49**, 994–999 (2011).

33. PAYNE, R. J. H. & JANSEN, V. A. A. Understanding Bacteriophage Therapy as a Density-dependent Kinetic Process. *J Theor Biol* **208**, 37–48 (2001).

34. Kumari, S., Harjai, K. & Chhibber, S. Bacteriophage versus antimicrobial agents for the treatment of murine burn wound infection caused by Klebsiella pneumoniae B5055. *J Med Microbiol* **60**, 205–210 (2011).

35. Kaur, P., Gondil, V. S. & Chhibber, S. A novel wound dressing consisting of PVA-SA hybrid hydrogel membrane for topical delivery of bacteriophages and antibiotics. *Int J Pharm* **572**, 118779 (2019).

36. Barrow, P. a. *et al.* T4 phages against Escherichia coli diarrhea: Potential and problems. *Virology* **14**, 209–211 (2004).

37. Suh, G. A. *et al.* Considerations for the Use of Phage Therapy in Clinical Practice. *Antimicrob Agents Chemother* **66**, (2022).

38. Morozova, V. V, Kozlova, Y. N., Ganichev, D. A. & Tikunova, N. V. Bacteriophage Treatment of Infected Diabetic Foot Ulcers. *Methods Mol Biol* **1693**, 151–158 (2018).

39. Chang, R. Y. K., Morales, S., Okamoto, Y. & Chan, H.-K. Topical application of bacteriophages for treatment of wound infections. *Transl Res* **220**, 153–166 (2020).

40. Steele, A., Stacey, H. J., de Soir, S. & Jones, J. D. The Safety and Efficacy of Phage Therapy for Superficial Bacterial Infections: A Systematic Review. *Antibiotics (Basel)* **9**, (2020).

41. Duplessis, C. A. & Biswas, B. A Review of Topical Phage Therapy for Chronically Infected Wounds and Preparations for a Randomized Adaptive Clinical Trial Evaluating Topical Phage Therapy in Chronically Infected Diabetic Foot Ulcers. *Antibiotics (Basel)* **9**, (2020).

42. Vonasek, E., Lu, P., Hsieh, Y. Lo & Nitin, N. Bacteriophages immobilized on electrospun cellulose microfibers by non-specific adsorption, protein–ligand binding, and electrostatic interactions. *Cellulose* **24**, 4581–4589 (2017).

43. Bach, M. S. *et al.* Filamentous bacteriophage delays healing of Pseudomonas-infected wounds. *Cell Rep Med* **3**, 100656 (2022).

44. de Vries, C. R. *et al.* A delayed inoculation model of chronic pseudomonas aeruginosa wound infection. *Journal of Visualized Experiments* **2020**, 1–6 (2020).

45. Sweere, J. M. *et al.* The Immune Response to Chronic Pseudomonas aeruginosa Wound Infection in Immunocompetent Mice. *Adv Wound Care (New Rochelle)* **9**, 35–47 (2020).

46. Fink, D. *et al.* Pseudomonas aeruginosa potentiates the lethal effect of intestinal ischemia-reperfusion injury: The role of in vivo virulence activation. *Journal of Trauma - Injury, Infection and Critical Care* **71**, (2011).

47. Burgener, E. B. & Bollyky, P. L. The Rational Design of Broadly Effective Phage Therapy Cocktails Against Bacterial Infections.

48. Wroe, J. A., Johnson, C. T. & García, A. J. Bacteriophage delivering hydrogels reduce biofilm formation in vitro and infection in vivo. *J Biomed Mater Res A* **108**, 39–49 (2020).

49. Wang, R., Yeh, Y. J., An, Y. N. & Virly. Engineering pH-sensitive erodible chitosan hydrogel composite containing bacteriophage: An interplay between hydrogel and bacteriophage against Staphylococcus aureus. *Int J Biol Macromol* **253**, 127371 (2023).

50. Tsai, C.-C. *et al.* Injectable, Shear-Thinning, Self-Healing, and Self-Cross-Linkable Benzaldehyde-Conjugated Chitosan Hydrogels as a Tissue Adhesive. *Biomacromolecules* **25**, 1084–1095 (2024).

51. Basu, S., Pacelli, S. & Paul, A. Self-healing DNA-based injectable hydrogels with reversible covalent linkages for controlled drug delivery. *Acta Biomater* **105**, 159–169 (2020).

52. Malone, M. *et al.* The prevalence of biofilms in chronic wounds: a systematic review and meta-analysis of published data. *J Wound Care* **26**, 1–5 (2017).

53. Davies, D. Understanding biofilm resistance to antibacterial agents. *Nat Rev Drug Discov* **2**, 114–122 (2003).

54. Costerton, J. W., Stewart, P. S. & Greenberg, E. P. Bacterial biofilms: a common cause of persistent infections. *Science (1979)* **284**, 1318–1322 (1999).

55. Vlamakis, H., Chai, Y., Beauregard, P., Losick, R. & Kolter, R. Sticking together: building a biofilm the Bacillus subtilis way. *Nat Rev Microbiol* **11**, 157–168 (2013).

56. Mann, E. E. & Wozniak, D. J. Pseudomonas biofilm matrix composition and niche biology. *FEMS Microbiol Rev* **36**, 893–916 (2012).

57. Parsek, M. R. & Singh, P. K. Bacterial biofilms: an emerging link to disease pathogenesis. *Annu Rev Microbiol* **57**, 677–701 (2003).

58. Uberoi, A., McCready-Vangi, A. & Grice, E. A. The wound microbiota: microbial mechanisms of impaired wound healing and infection. *Nat Rev Microbiol* (2024) doi:10.1038/s41579-024-01035-z.

59. Shafigh Kheljan, F. *et al.* Design of Phage-Cocktail–Containing Hydrogel for the Treatment of Pseudomonas aeruginosa–Infected Wounds. *Viruses* **15**, 803 (2023).

60. Patpatia, S. *et al.* Rapid hydrogel-based phage susceptibility test for pathogenic bacteria. *Front Cell Infect Microbiol* **12**, 1032052 (2022).

61. Kim, H. Y., Chang, R. Y. K., Morales, S. & Chan, H. K. Bacteriophage-delivering hydrogels: Current progress in combating antibiotic resistant bacterial infection. *Antibiotics* **10**, 1–17 (2021).

62. Kalelkar, P. P., Riddick, M. & García, A. J. Biomaterial-based antimicrobial therapies for the treatment of bacterial infections. *Nat Rev Mater* **7**, 39–54 (2022).

63. Bai, H. *et al.* Phage-Based antibacterial hydrogels for bacterial targeting and Ablation: Progress and perspective. *European Journal of Pharmaceutics and Biopharmaceutics* **198**, 114258 (2024).

64. Barros, J. A. R. *et al.* Encapsulated bacteriophages in alginate-nanohydroxyapatite hydrogel as a novel delivery system to prevent orthopedic implant-associated infections. *Nanomedicine* **24**, (2020).

65. Shen, H. Y. *et al.* Controlled-release of free bacteriophage nanoparticles from 3D-plotted hydrogel fibrous structure as potential antibacterial wound dressing. *Journal of Controlled Release* **331**, 154–163 (2021).

66. Chang, R. Y. K., Okamoto, Y., Morales, S., Kutter, E. & Chan, H. K. Hydrogel formulations containing non-ionic polymers for topical delivery of bacteriophages. *Int J Pharm* **605**, 120850 (2021).

67. Agarwal, R. *et al.* Inhaled bacteriophage-loaded polymeric microparticles ameliorate acute lung infections. *Nat Biomed Eng* **2**, 841–849 (2018).

68. Bean, J. E. *et al.* Triggered release of Bacteriophage K from agarose/hyaluronan hydrogel matrixes by staphylococcus aureus virulence factors. *Chemistry of Materials* **26**, 7201–7208 (2014).

69. Rubalskii, E. *et al.* Fibrin glue as a local drug-delivery system for bacteriophage PA5. *Sci Rep* **9**, 3–10 (2019).

70. Ren, H. *et al.* Injectable, self-healing hydrogel adhesives with firm tissue adhesion and on-demand biodegradation for sutureless wound closure. *Sci Adv* **9**, eadh4327 (2023).

71. Roth, J. G. *et al.* Tunable hydrogel viscoelasticity modulates human neural maturation. *Sci Adv* **9**, eadh8313 (2023).

72. Sharma, P. K. & Singh, Y. Glyoxylic Hydrazone Linkage-Based PEG Hydrogels for Covalent Entrapment and Controlled Delivery of Doxorubicin. *Biomacromolecules* **20**, 2174–2184 (2019).

73. Hua, Y. *et al.* Adaptable to Mechanically Stable Hydrogels Based on the Dynamic Covalent Cross-Linking of Thiol-Aldehyde Addition. *ACS Macro Lett* **8**, 310–314 (2019).

74. Liu, D. *et al.* The safety and toxicity of phage therapy: A review of animal and clinical studies. *Viruses* **13**, 1–20 (2021).

75. Chung, K. M., Nang, S. C. & Tang, S. S. The Safety of Bacteriophages in Treatment of Diseases Caused by Multidrug-Resistant Bacteria. *Pharmaceuticals* **16**, (2023).

76. Zyman, A., Górski, A. & Międzybrodzki, R. Phage therapy of wound-associated infections. *Folia Microbiol (Praha)* **67**, 193–201 (2022).

77. El Haddad, L., Harb, C. P., Gebara, M. A., Stibich, M. A. & Chemaly, R. F. A Systematic and Critical Review of Bacteriophage Therapy Against Multidrug-resistant ESKAPE Organisms in Humans. *Clinical Infectious Diseases* **69**, 167–178 (2019).

78. Pirnay, J. P. *et al.* Personalized bacteriophage therapy outcomes for 100 consecutive cases: a multicentre, multinational, retrospective observational study. *Nat Microbiol* **9**, (2024).

79. Chadha, P., Katare, O. P. & Chhibber, S. In vivo efficacy of single phage versus phage cocktail in resolving burn wound infection in BALB/c mice. *Microb Pathog* **99**, 68–77 (2016).

80. Dharmaraj, T. *et al.* Rapid assessment of changes in phage bioactivity using dynamic light scattering. *PNAS Nexus* **2**, (2023).

81. Chen, J. S., Longaker, M. T. & Gurtner, G. C. Murine models of human wound healing. *Methods Mol Biol* **1037**, 265–74 (2013).

82. Sweere, J. M. *et al.* Bacteriophage trigger antiviral immunity and prevent clearance of bacterial infection. *Science (1979)* **363**, (2019).

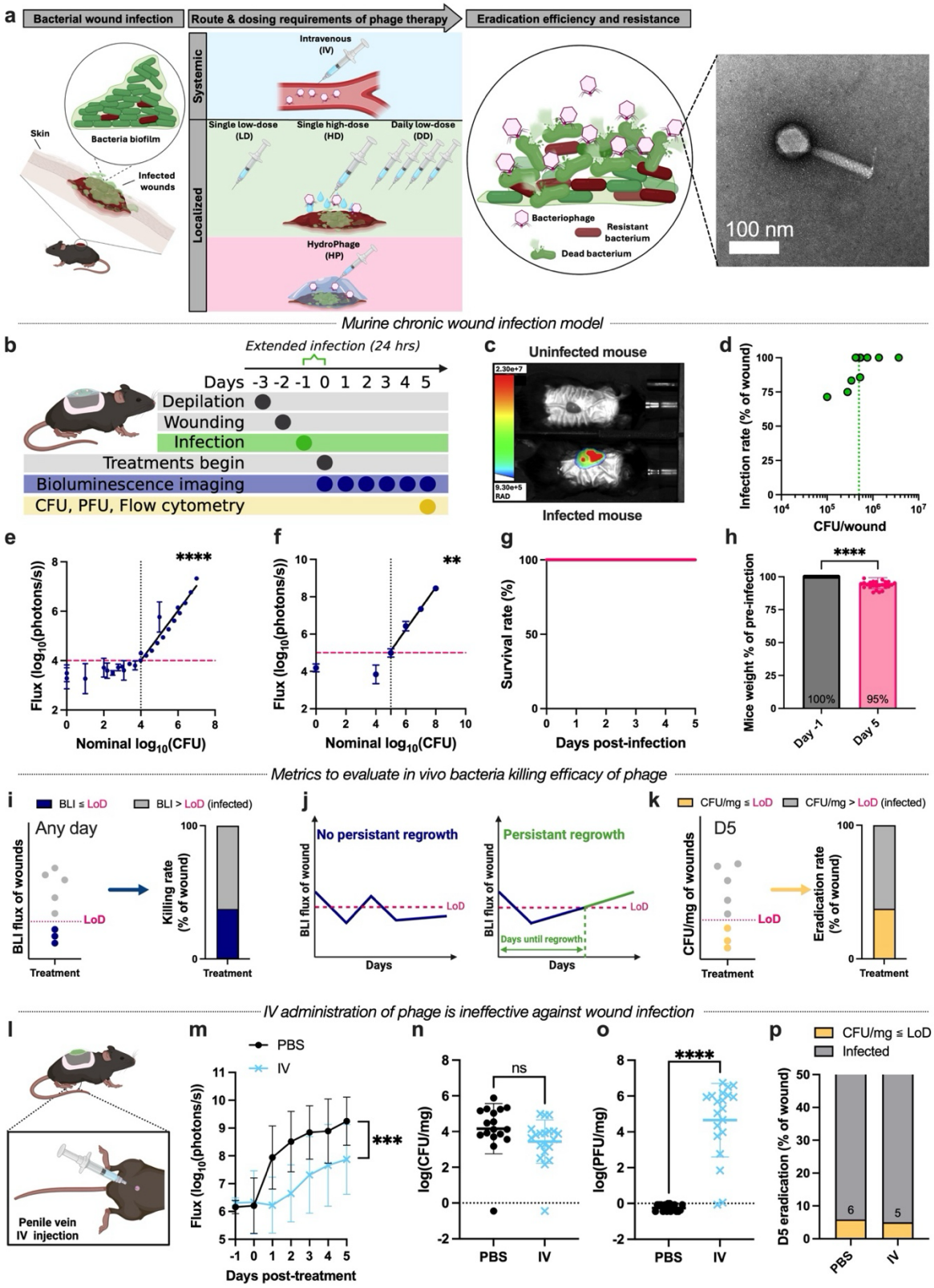

Fig. 1. Intravenous (IV) phage therapy (PT) is ineffective against *Pa* wound infection. a, illustration of the research summary (left), and PAML-31-1 phage visualized using transmission

electron microscopy (TEM) (right). Scale bar = 100 nm. **b-h,** Development of BLI and murine wound infection model**.** Illustration of the timeline of murine wound model (**b**); the representative BLI image of uninfected (top) and infected (bottom) mice, where color bar indicates the flux intensity (**c**); the wound infection rate at different inoculation density of Xen41 (**d**); bioluminescent signal and nominal CFU correlations *for* Xen41 *in vitro* (Pearson r = 0.953, P < 0.001; R^2 = 0.889) (**e**) and *in vivo* (Pearson r = 0.996, P = 0.0043; R^2 = 0.977) (**f**); mice survival rate after inoculation with 5 x 10^5 CFU/wound Xen41 up to 5 days post-infection, n=20 (**g**); and the percentage of weight to pre-infection weight for mice on Day 5 after inoculation with 5 x 10^5 CFU/wound Xen41, n=29 (**h**), **i**,**j**,**k**, Metrics used to evaluate the *in vivo* bacterial killing efficacy of phage treatments. The killing rate defined as the percentage of wounds having bioluminescent flux signal below limit of detection (LoD) of given day (**i**); the persistent growth rate defined as the percentage of wounds where bioluminescent flux signal remained higher than LoD (**j**); and the eradication rate defined as the percentage of wounds CFU lowered than LoD (**k**). **l**,**m**,**n**,**o**,**p**, Evaluation of *in vivo* efficacy of IV phage treatment. Illustration demonstrates the penile vein injection for IV phage treatment (**l**); the time evolution of bioluminescent flux signal comparing IV versus PBS control treatment (**m**); bacterial burden (CFU/mg) (**n**) and phage counts (PFU/mg) (**o**) recovered from harvested mice wound tissue; and the eradiation rate (**p**), n=17 for PBS and n= 17 for IV. Schematics in (**a**), (**b**) and (**l**) were generated with BioRender. Data are presented as mean ± S.D. Unpaired two-tailed Student's *t*-test for (**h**), (**n**), and (**o**). Two-way ANOVA with mixed-effects model and Geisser-Greenhouse correction where day and treatment as fixed effects and mouse ID as a random effect and analyzed from Day 0 to 5 for (**m**) (** $P \leq 0.01$, *** $P \leq 0.001$, **** $P \leq 0.0001$).

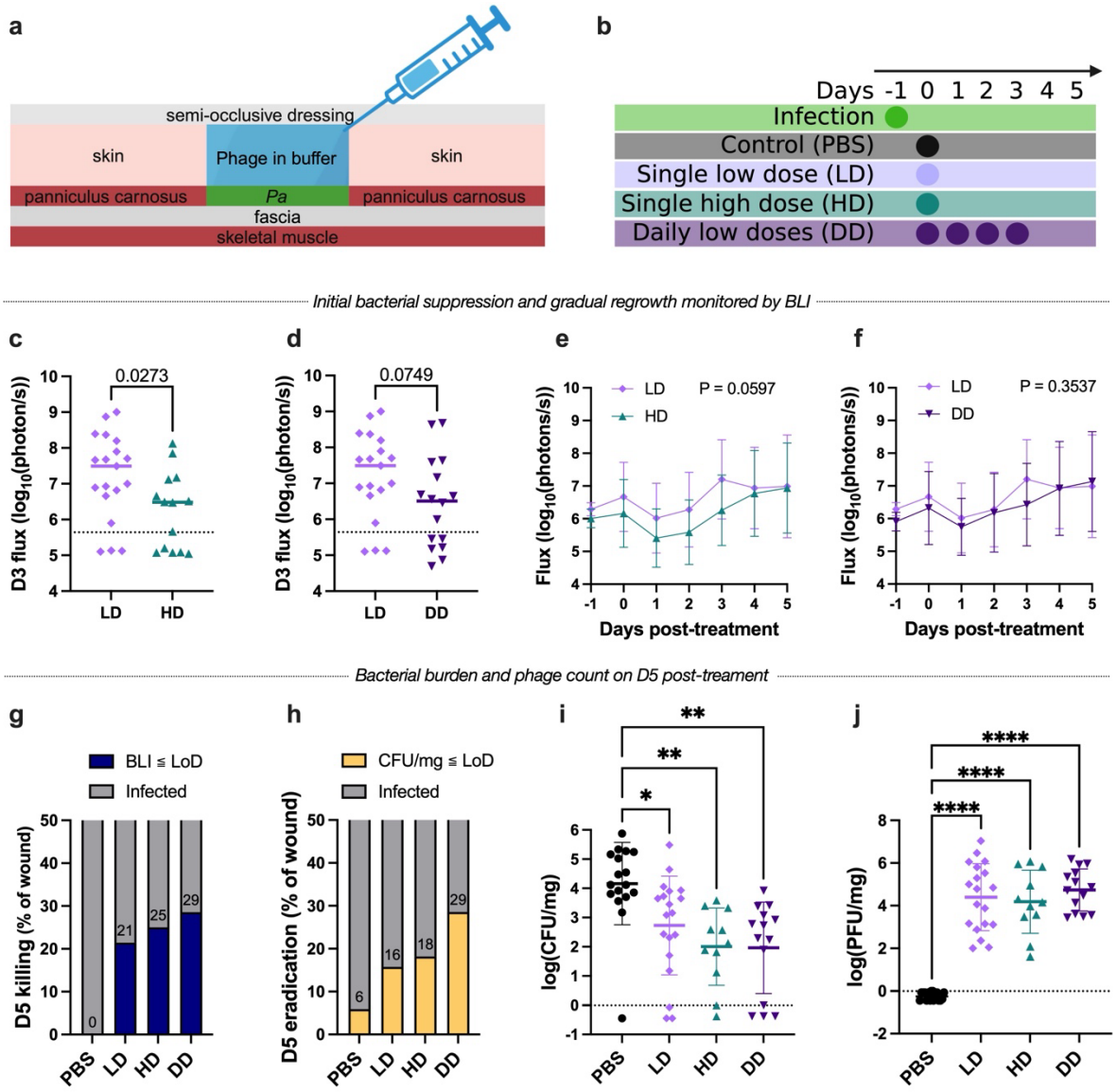

Fig. 2. Local phage delivery reduce bacterial burden. a, Illustration of how mice receive liquid phage treatments by topical injection under Tegaderm dressing. **b**, Illustration of the murine wound study to compare the efficacy of PT with different dosing concentration and frequency. **c**,**d**, The bioluminescent flux signal on D3 post-treatment comparing HD versus LD (**c**) and DD versus LD (**d**). **e**,**f**, The time evolution of bioluminescent flux signal comparing DD versus LD treatments (**e**) and DD versus LD treatments (**f**). The bacterial killing rate at the end of the study, Day 5 post-treatment (**g**); n=17 for PBS, n=14 for LD, n=12 for HD, and n=14 for DD. **h**,**i**,**j**, Endpoint characterization of harvested mice wound tissue. The eradiation rate (**h**); bacterial burden (CFU/mg) (**i**) and phage counts (PFU/mg) (**j**) recovered from harvested mice wound tissue, n=17 for PBS, n=19 for LD, n=11 for HD, and n=14 for DD. Schematics in (**a**), (**b**) were generated with BioRender. Data are presented as mean ± S.D. Unpaired two-tailed Student's *t*-test for (**c**) and (**d**). Two-way ANOVA with mixed-effects model and Geisser-Greenhouse correction where day and treatment as fixed effects and mouse ID as a random effect and analyzed from Day 0 to 5 for (**e**) and (**f**). One-way ANOVA with Tukey's post-hoc test for (**i**) and (**j**) (* $P \leq 0.05$, ** $P \leq 0.01$, **** $P \leq 0.0001$).

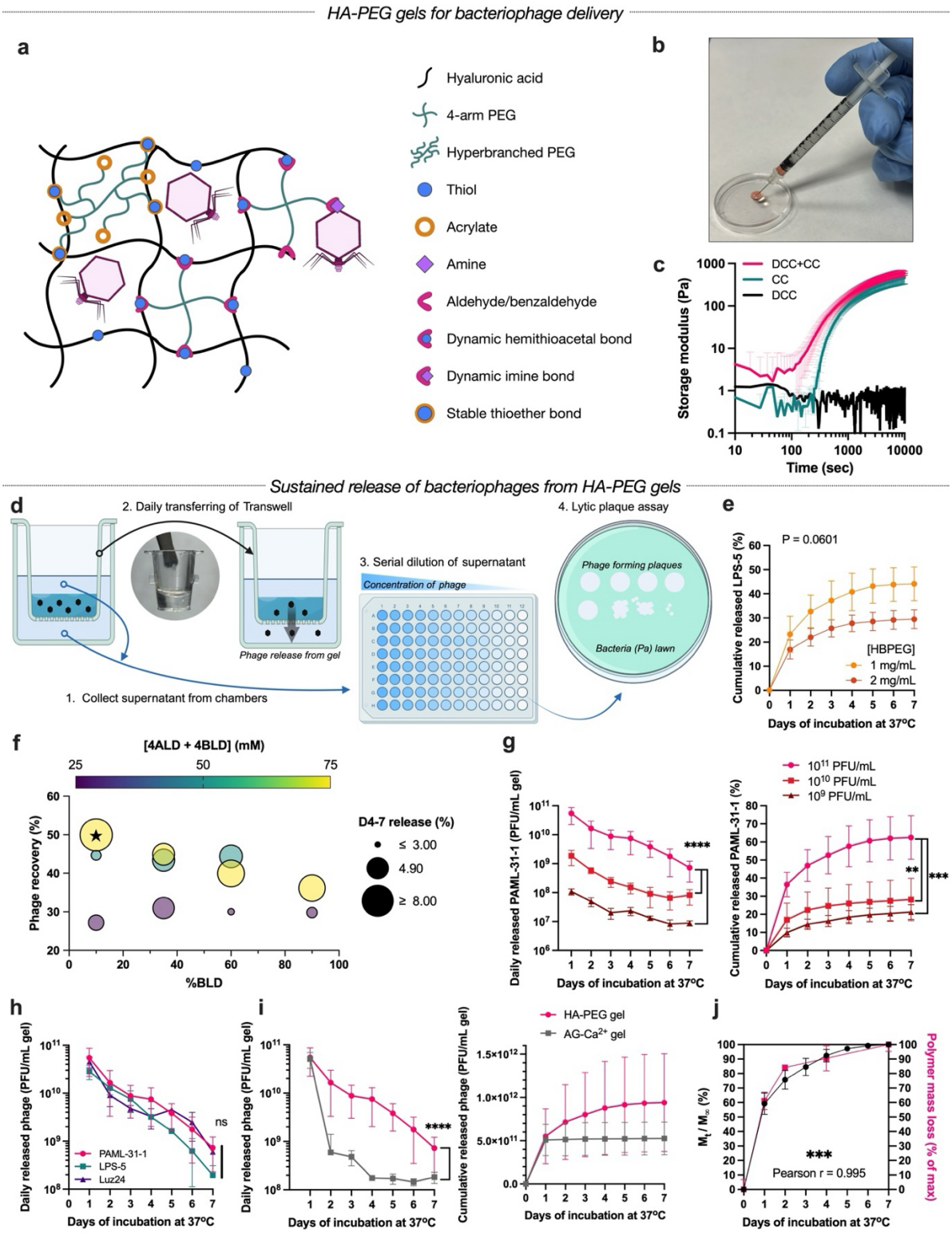

Fig. 3. HA-PEG hydrogels with dynamic covalent and static covalent crosslinks for sustained delivery of high-dose bacteriophage. a, Schematic of hyaluronic acid (HA)- and polyethylene glycol (PEG)-based hydrogel (HA-PEG) crosslinking chemistries. Covalent thioether

crosslinks are formed between thiolated-HA (HA-SH) and hyperbranched PEG multi-acrylate (HBPEG). Dynamic covalent hemithioacetal crosslinks are formed between HA-SH with either 4-arm PEG-aldehyde (4ALD) or benzaldehyde (4BLD). Amines presented on the surface of phages could theoretically bind to aldehyde/benzaldehyde through dynamic covalent imine bonds. **b**, Image of HA-PEG hydrogel injected through a 28G needle. **c**, The storage modulus of hydrogels with both dynamic covalent crosslinking and covalent crosslinking (DCC+CC, magenta), covalent crosslinking alone (CC, green), and dynamic covalent crosslinking alone (DCC, black). Hydrogel formulations: 7 mg/mL HA-SH, 4 mg/mL HBPEG, and 75 mg/mL of 4-arm PEGs with 10% 4BLD and 90% 4ALD for DCC+CC gel, n=4; 7 mg/mL HA-SH and 4 mg/mL HBPEG for CC gel, n=3; 7 mg/mL HA-SH and 75 mg/mL of 4-arm PEGs with 10% 4BLD and 90% 4ALD for DCC gel, n=1. **d**, Schematic of the transwell-release assay to quantify phage release from HA-PEG hydrogel daily. **e**, HBPEG of 1 mg/mL led to a higher percentage of phage recovery compared to 2 mg/mL; n=3 for each formulation. **f**, The HA-PEG hydrogel contained 5 mg/mL of HA-SH and 1 mg/mL of HBPEG, and the 4-arm PEGs concentration and %BLD were varied to explore the optimal hydrogel formulation with the highest percentage of recovery and sustained release. Sustained release was defined as the cumulative phage release from Day 4 to 7, indicated by the size of the dots; n=1 for each formulation. The star sign indicates the chosen hydrogel formulation for the rest of the study. **g**. Quantification of daily and cumulative release of PAML-31-1 phage out of HA-PEG hydrogel with different encapsulation titres: 10^{11}, 10^{10}, and 10^{9} PFU/mL; n=8, 3, and 3, respectively. **h**, Quantification of daily release of different phages—PAML-31-1, LPS-5, and Luz24—from HA-PEG hydrogel with encapsulation titre of 10^{11} PFU/mL; n=8, 4, and 2, respectively. **i**, Comparison of the daily and cumulative release of phage from HA-PEG hydrogel versus an ionically crosslinked alginate hydrogel (AG-Ca^{2+}) with encapsulation titre of 10^{11} PFU/mL; n=8 and 4, respectively. **j**, Close correspondence between the percentage of maximum phage release, defined as the ratio of cumulative phage release at given time point (M_t) to the endpoint maximum cumulative release (M_∞), and the mass loss of HA-PEG hydrogel, defined as the percentage of mass loss to the maximum mass loss; n=8 and 3, respectively. The PAML-31-1 phage release from HA-PEG gel data presented in (**h-j**) are referenced from the 10^{11} PFU/mL data in (**g**). Schematics in (**a**), (**d**) generated with BioRender. Data are presented as mean ± S.D for (**c**), (**e**), (**g**), (**h**), and (**j**). Repeated measures two-way ANOVA with Geisser-Greenhouse correction for (**e**), (**g**), (**h**) and (**i**) (PAML-31-1 vs LPS-5). Two-way ANOVA with mixed-effects model and Geisser-Greenhouse correction where phage type and day as fixed effects and gel ID as a random effect for (**i**) (PAML-31-1 vs Luz24 and LPS-5 vs Luz24). Bonferroni's correction for multiple comparisons for (**g**) and (**h**). Pearson correlation for (**j**). (** $P \leq 0.01$, *** $P \leq 0.001$, **** $P \leq 0.0001$).

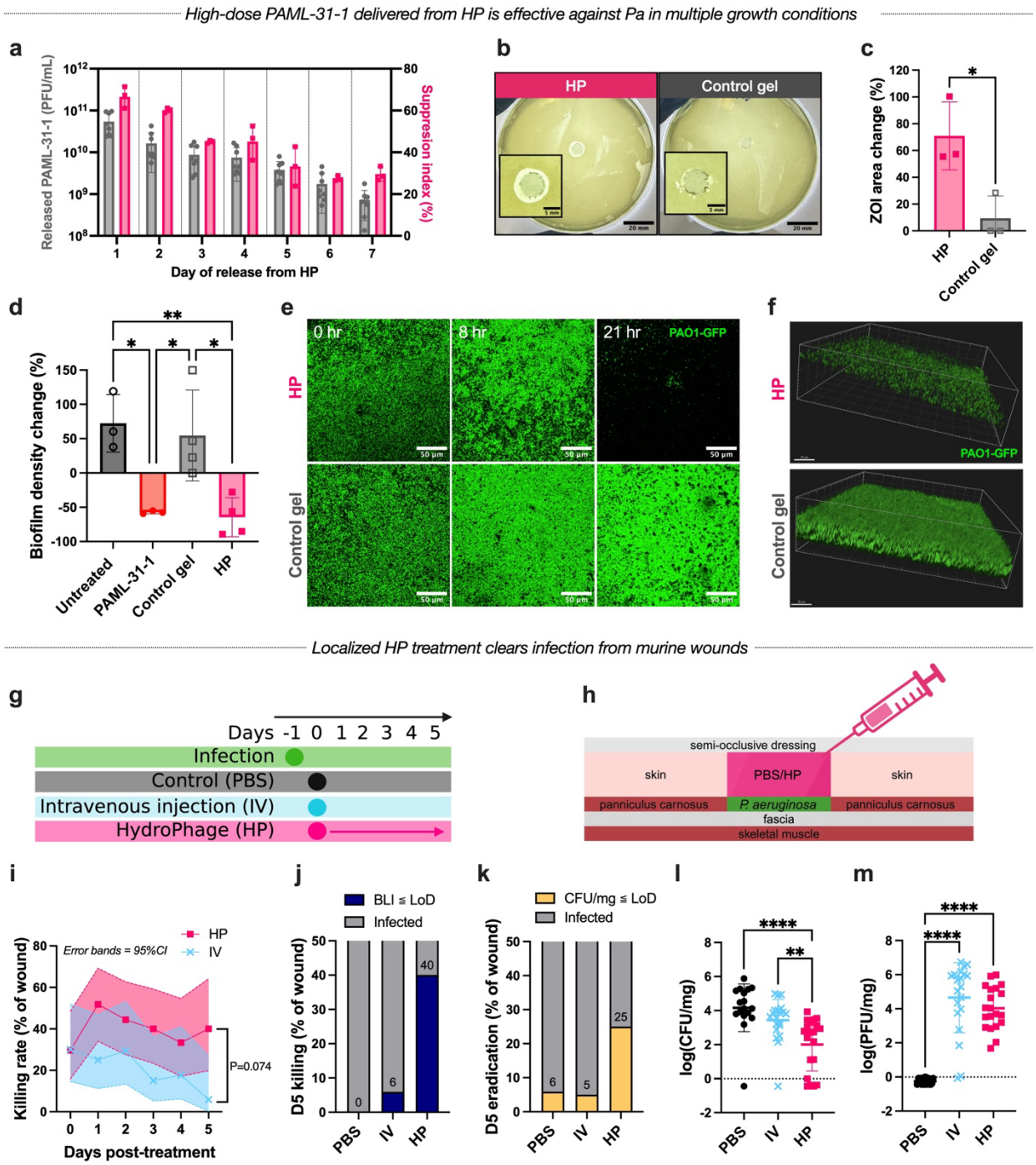

Fig. 4. Phage-delivering HA-PEG hydrogels (HydroPhage, HP) suppress *Pa* in multiple growth mode *in vitro* and clears wound infections *in vivo*. a, Quantification of suppression index (SI%) (n=3) against Xen41 by planktonic suppression assay (PSA) with the PAML-31-1 titre (n=8) released from HP in transwell-release assay daily. The daily released PAML-31-1 titre data are referenced from **Figure 3g**. **b**,**c**, The zone of inhibition (ZOI) formed by HP and control gel at 24 hours of gel placement on *Pa* lawn. The representative images of HP and control gel on *Pa* lawn (**b**), and quantification of change in ZOI area at 24 hours as a percent of initial area of hydrogel (**c**); n=3 each. **d**,**e**,**f**, PAO1-GFP biofilm was formed on the surface of top agar and

treated with untreated control, PAML-31-1 phage in media, control gel or HP for 21 hours; n=3, 3, 4, and 4, respectively. The quantification of biofilm density changes (**d**), representative confocal images of biofilm incubated with HP and control gel treatments over hours (**e**), and the 3D rendering of biofilm at 21 hours (**f**). **g**, Illustration of a murine wound infection study to test the efficacy of HP and IV phage injection treatments. **h**, Illustration of how mice receive HP or PBS control treatment by topical injection under Tegaderm dressing. **i**,**j**, The real-time monitoring of bacterial burden with BLI. The time evolution of bacterial killing rate (**i**), and the killing rate at the end of the study, Day 5 post-treatment (**j**); n=17 for PBS, n=17 for IV, and n=15 for HP. **k**,**l**,**m,** Endpoint characterization of harvested mice wound tissue. The eradication rate defined as the percentage of wounds having bacterial burden below LoD (**k**). and bacterial burden (CFU/mg) (**l**) and phage counts (PFU/mg) (**m**) recovered; n=17 for PBS, n=20 for IV, and n=20 for HP. Data are presented as mean ± S.D except as mean ± 95% confidence interval (CI) for (**i**). Unpaired two-tailed Student's t-test for (**c**). One-way ANOVA with Tukey's post-hoc test for (**d**), (**l**), and (**m**). Generalized linear mixed model with day and treatment as fixed effects and mouse ID as a random effect, using a binomial distribution and analyzed from Day 0 to 5 for (**i**). Scale bars: 20 mm for (**b**) and 5 mm for the inset, 50 μm for (**e**), and 30 μm for (**f**). (* $P \leq 0.05$, ** $P \leq 0.01$, **** $P \leq 0.0001$).

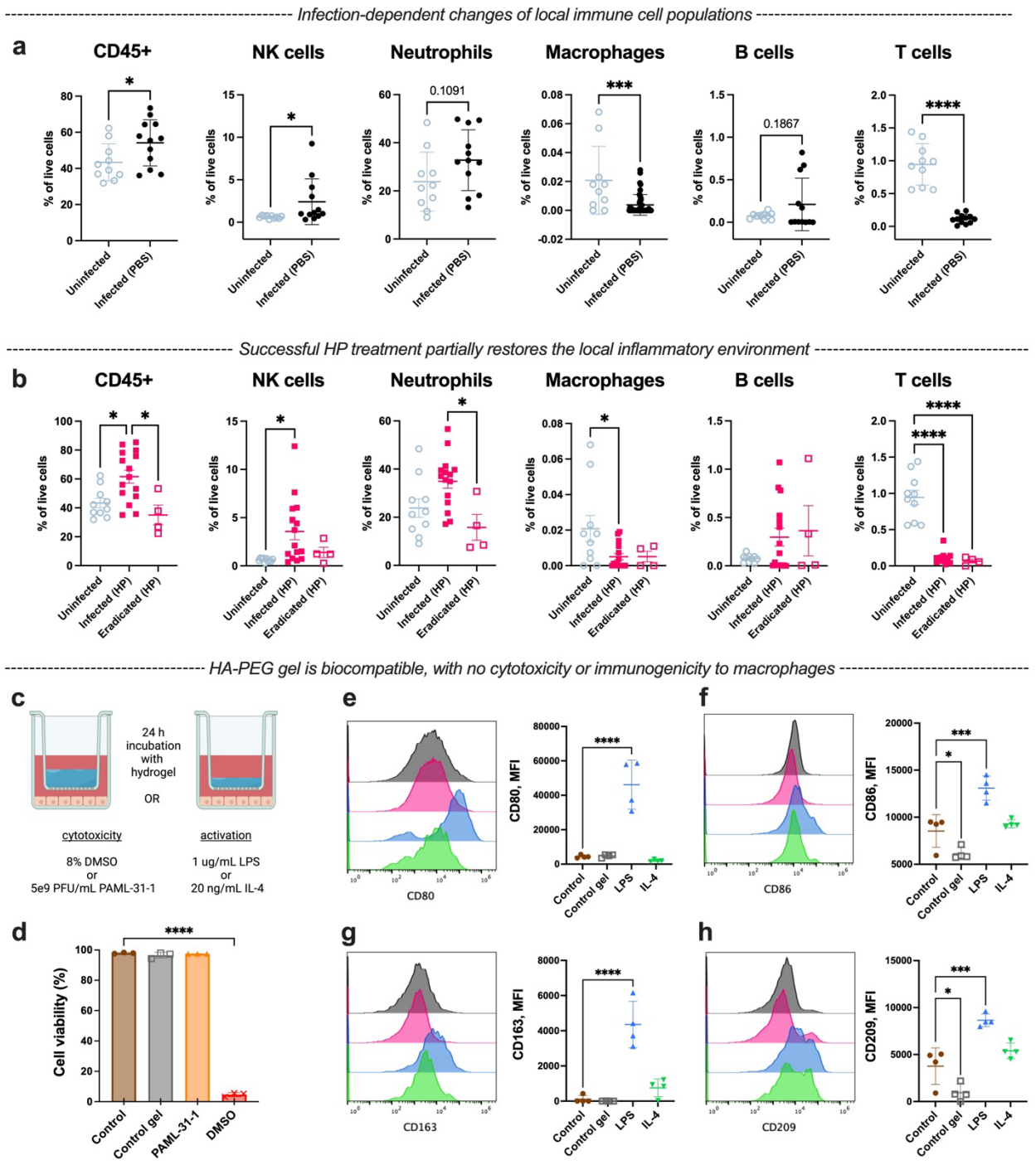

Fig. 5. HydroPhage is biocompatible and treatment with hydrophage partially reverses infection-dependent changes of skin-associated immune cell populations. **a**, The abundance of CD45^{+}, natural killer (NK) cells, neutrophils, macrophages, B cells, and T cells in uninfected mouse wounds versus wounds infected with *Pa* and treated with PBS; n=10 for uninfected mice and n=12 for infected (PBS treated) mice. **b**, The abundance of CD45^{+} cells, NK cells, neutrophils, macrophages, B cells, and T cells in uninfected mice wounds versus mice treated with HP, where the treatment results were stratified by outcome as either infected or eradicated; n=10 for uninfected mice, n=15 for infected (HP-treated) mice, and n=4 for eradicated

(HP-treated) mice. See **Extended Data Figure 6** for gating strategy and cell definitions. **c**, Schematic of transwell exposure assay of cytotoxicity and macrophage activations. **d**, Cytotoxicity of HA-PEG gel (control gel) and PAML-31-1 phage to RAW264.7 cells using transwell system; n=3 each. **e**-**h**, Representative histograms (left) and median fluorescence intensity (MFI) of fluorochrome-conjugated antibodies against classical M1 (CD80, CD86) and M2 (CD163, CD209) markers in RAW264.7 cells after treatment with media only control, control gel in transwell system, 1 ug/mL *E. coli* LPS, or 20 ng/mL mIL-4; n=4 each. Data are mean ± S.D. Unpaired two-tailed Student's t-test for (**a**). Ordinary one-way ANOVA with Tukey post-hoc tests for (**b**) and with Dunnett post-hoc tests versus PBS control group for (**d**-**h**) (* $P \leq 0.05$, *** $P \leq 0.001$, **** $P \leq 0.0001$).

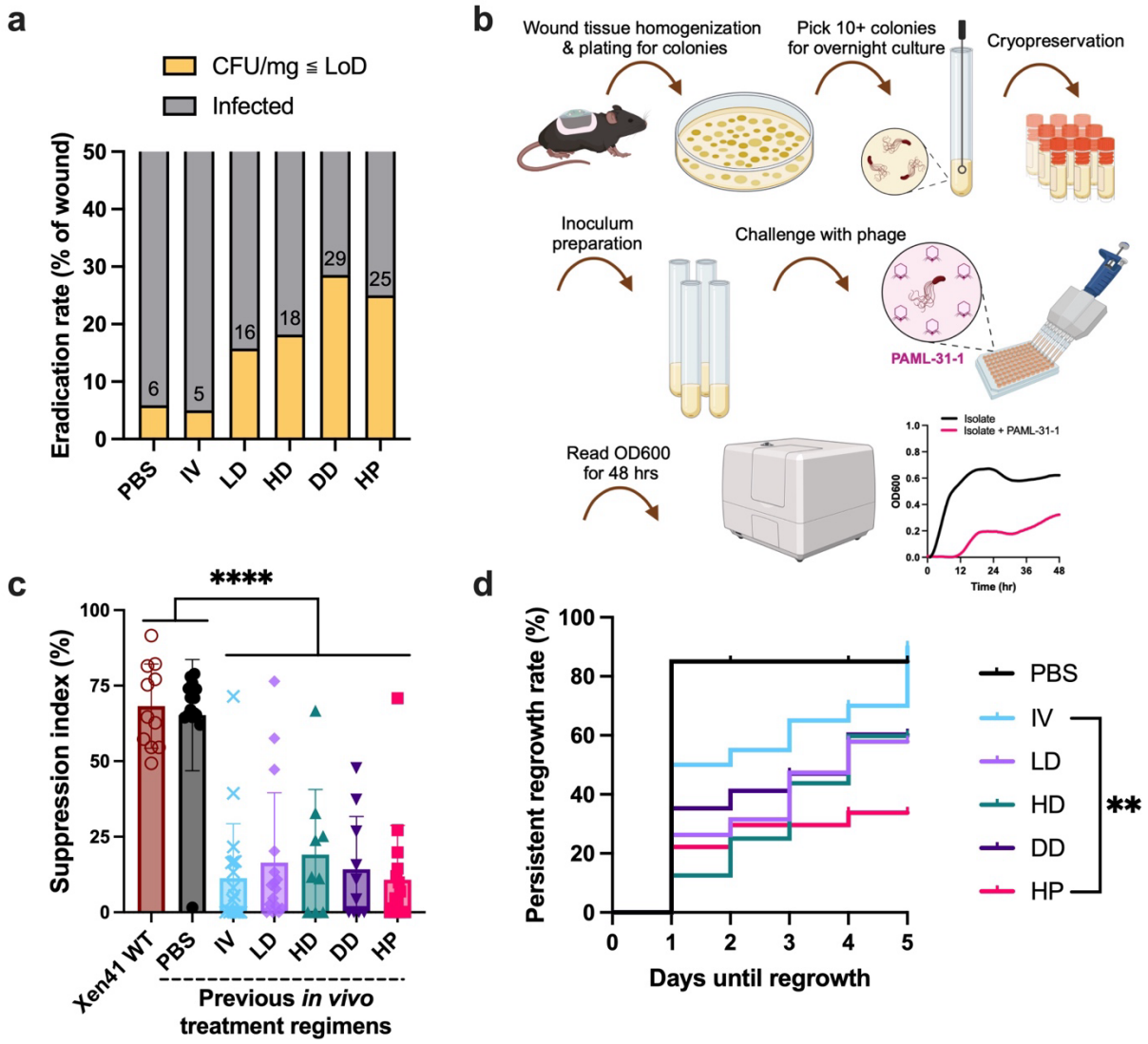

Fig. 6. Development of phage resistance from phage treatment is independent of treatment, dosing, route, and efficacy. a, Summary of eradication rates by phage treatments investigated from **Figures 2h and 4k**. The isolates from endpoint infected wound were used for downstream resistance characterization. **b,** Schematic of PSA for the mice wound isolates to characterize bacteria resistance after prior PAML-31-1 treatment regimens, compared to PBS-treated control and wild-type Xen41. **c,** Quantification of SI% for PAML-31-1 against Xen41 WT and wound isolates with previous *in vivo* treatment regimens; n=11 for Xen41 WT, n=15 for PBS, n=19 for IV, n=16 for v, n=9 for HD, n=10 for DD, and n=16 for HP. **d**, The persistent regrowth rate of different treatment regimens, HP is the only localized treatment presents significant difference with IV treatment (P = 0.0064). Schematic in (**b**) was generated with BioRender. Data are mean ± S.D. One-way ANOVA with Tukey's post-hoc test for (**c**). Log-rank test with Bonferroni's correction for multiple comparison for (**d**). (** $P \leq 0.01$, **** $P \leq 0.0001$).